

Research Article

Thermal degradation kinetic studies of polypropylene (PP)/titanium dioxide (TiO₂) composites

 Krishna Prasad Rajan^{a,*}, Mohammed Rafic^b, Selvin P. Thomas^{a,*}
^a Department of Chemical Engineering, Yanbu Industrial College, P.O. Box 30436, Yanbu Industrial City 41912, Saudi Arabia

^b Department of General Studies, Yanbu Industrial College, P.O. Box 30436, Yanbu Industrial City 41912, Saudi Arabia

ARTICLE INFO

Keywords:

 Polypropylene
 Titanium dioxide
 Composites
 Thermal degradation kinetics
 Iso-conversional methods
 Kinetic models

ABSTRACT

The degradation kinetics of polypropylene (PP) composites reinforced with titanium dioxide (TiO₂) microparticles were investigated using various kinetic models. The composites were prepared through a twin-screw extrusion process by varying the filler loading up to 30 wt%. The thermal degradation studies were conducted by using a thermogravimetric analyzer (TGA) at four different heating rates. The activation energies of the degradation of the composites were calculated using different model equations such as Friedman, Kissinger-Akahira-Sunose (KAS), Ozawa-Flynn, Wall (OFW), and Starink. The Horowitz and Metzger method revealed an increasing trend in activation energy with higher filler loadings, attributed to enhanced barrier properties, improved dispersion, increased thermal stability, and the formation of protective layers. The Coats-Redfern method indicated a transition in the thermal degradation mechanism from the contracting sphere model to the contracting cylinder model with the incorporation of TiO₂. The Criado model highlighted a shift from the Avrami-Erofeev equation (A₂ mechanism) to the power law-contracting cylinder mechanism (R₂) in PP/TiO₂ composites, driven by improved nucleation and growth, filler-matrix interactions, and barrier effects. These findings demonstrate that the incorporation of TiO₂ particles significantly enhances the thermal stability and alters the degradation mechanisms of PP composites, providing valuable insights for the development of advanced composite materials with improved thermal properties.

1. Introduction

Polypropylene (PP) is an economic choice among commodity thermoplastics for superior applications that require exceptional mechanical properties, thermal properties, chemical, and weather resistance along with excellent processability characteristics [1]. The properties of this polyolefin type of thermoplastic can greatly be improved by blending with other polymers and also by incorporating several reinforcing and non-reinforcing types of fillers. Elastomer-modified grades of PP, thermoplastic elastomers of PP, glass fiber-reinforced PP, biofiber-reinforced PP, particulate filler-reinforced PP, etc. are examples for such commercial types of modified PP readily available for diversified applications [2].

However, there exists a serious limitation for polymeric materials in terms of thermal and oxidative stability and thermal endurance, which confines their applications in high-temperature environments [3]. Various techniques were adopted to overcome this limitation and among them, reinforcing the polymer matrix with a high-temperature resistant mineral filler is an attractive and economically feasible approach. Titanium dioxide, calcium carbonate, mica, silica, talc, clay, calcium sulfate,

and alumina trihydrate are typical examples of commonly used mineral fillers in plastics [4]. Natural mineral-reinforced polymer composites offer enhanced mechanical properties, dimensional stability, hardness, stiffness, barrier properties, and flame retardance in addition to their increased high-temperature stability [5].

Titanium dioxide (TiO₂) is a promising mineral filler that is widely used as a white pigment in paint formulations due to its color brightness and hiding effects [6]. In polymer composites, TiO₂ improves the thermal stability of the base matrix, offers flame retardancy, and acts as an antioxidant in addition to its effect as a reinforcing filler [7,8]. TiO₂ is widely utilized in polymer composites due to its favorable physico-chemical properties, such as high refractive index, photocatalytic activity, dielectric properties and thermal stability [9]. When incorporated into polymer matrices, TiO₂ particles significantly enhance mechanical strength, UV resistance, and thermal durability. Their incorporation increases interfacial surface area, which improves load transfer and alters polymer crystallinity, resulting in superior composite performance even at low filler concentrations. Moreover, TiO₂'s low band gap and surface reactivity make it ideal for applications in environmental remediation, biomedical devices, and smart coatings [10]. Surface mod-

* Corresponding authors.

E-mail addresses: rajankp@rcjy.edu.sa (K.P. Rajan), stthomas@rcjy.edu.sa (S.P. Thomas).
<https://doi.org/10.1016/j.chphma.2025.09.003>

Received 18 March 2025; Received in revised form 12 September 2025; Accepted 17 September 2025

Available online 16 October 2025

2772-5715/© 2025 The Authors. Publishing Services by Elsevier B.V. on behalf of KeAi Communications Co. Ltd. This is an open access article under the CC BY license (<http://creativecommons.org/licenses/by/4.0/>)

ification of TiO₂ further tailors its compatibility with various polymer systems, optimizing dispersion and interfacial bonding. Mina et al. [11] prepared a composite of isotactic polypropylene (iPP) with TiO₂ by extrusion and compression molding techniques and studied the effect of TiO₂ on the crystal structure of iPP in addition to the improvements in physico-mechanical properties of the composites. An interesting observation is that the three-phase crystalline system (α , β , γ) of the base iPP changed to a single phase (α form) with the incorporation of TiO₂. Sirirat et al. [8] prepared PP/TiO₂ composites by melt extrusion techniques and reported that when TiO₂ of particle size 130 nm was incorporated into the PP matrix at a screw speed of 50 rpm with 2 mixing cycles significantly improved the dispersion of filler particles in the PP matrix and thereby improved the tensile and impact properties of the composites. The incorporation of nanoparticles of TiO₂ into the PP matrix was carried out by Esthappan and co-workers [12]. It was reported that the thermal ageing characteristics and thermal degradation behaviors of PP were improved with the incorporation of TiO₂. The same research group prepared nanofibers of PP/TiO₂ composites following melt spinning and drawing techniques. The nano-fibers exhibited superior mechanical and thermal properties compared with those of neat PP [13]. The hydrophilic character of TiO₂ was utilized in PP-based composite membranes for enhancing the polarity and thereby improving the electrolyte uptake properties of these microporous membranes [14]. Uzun et al. prepared nano TiO₂-reinforced PP and reported a reduction in water absorption and an improvement in physico-mechanical properties of the composites with the increase in the TiO₂ loading [15]. Another recent study reported the effect of dicarboxylic acid-modified TiO₂ nanoparticles on the β -nucleation efficiency of the isotactic PP composites [16]. PP composites were prepared by adding TiO₂, graphene nanoplatelets, and their hybrids in various ratios along with a fixed amount of compatibilizer composites, and the mechanical, thermal, and morphological properties of the composites were studied by Kumar et al. [17]. The good interfacial adhesion between the filler and PP matrix led to significant improvements in tensile modulus, thermal degradation temperature, and melting temperature especially in the hybrid composites. Junaedi et al. attempted to study the effect of adding nano TiO₂ in different weight percentages to different melt flow index PP matrices on the physical and morphological properties in comparison with carbon fiber and graphite nanoplatelets [18].

A thorough understanding of the thermal degradation kinetics and mechanism is very much essential to predicting the behavior of PP/TiO₂ composites in applications that require high temperatures. In addition, the pyrolysis-combustion process as an energy recovery route is gaining popularity due to the environmental regulations in many countries [19]. Thermal degradation of polymers and composites comprises complex physical and chemical changes and associated complex reactions. Exposure to high temperatures often results in the breaking of polymer chains and leads to a rapid reduction in molecular weight. It also leads to the formation of gaseous products and residues [20]. The careful design of the pyrolysis process necessitates a detailed and systematic understanding of the degradation kinetics [21,22]. Various mathematical models are in use that describe the pyrolysis kinetics and mechanism of thermal degradation of polymer composites. These models help researchers to understand the degradation mechanism in a better way and thereby help in predicting the thermal behavior of materials under elevated temperatures.

Thermal degradation kinetics of PP-based systems were studied by various researchers as per the literature available. An interesting study is reported by Das and Tiwari in which they studied the thermal degradation behavior of four polymers low and high-density polyethylene (LDPE and HDPE), PP, and polylactic acid (PLA) under seven different heating rates and used isoconversional models [23]. Criado's masterplots were developed to predict the reaction models ($f(\alpha)$). Activation energy and pre-exponential factors were computed using Friedman, Kissinger-Akahira-Sunose, Ozawa-Flynn, and Wall (OFW), Starink, and advanced isoconversional method (AIC) models/methods. It was found that each

polymer degradation is different from each other. Even then it is a good report to understand the degradation mechanism of PP under different conditions. Another interesting study reported the kinetics behavior of three types of milk bottles made up of HDPE and PP plastics of which PP were transparent and non-transparent [24]. PP bottles were less stable than HDPE due to the structural difference. Isoconversional integral Flynn-Wall-Ozawa (FWO), Starink (SK), and Vyazovkin-Dollimore (VD) methods, and differential Friedman (FD) methods were utilized to study the mechanism. The kinetic parameters as well as the thermodynamic properties with respect to the conversion factors reflected the mechanism of degradation of the three different polyolefins in detail.

Thermal degradation kinetics of PP with alkali and saline-treated sugarcane bagasse fibers was done and found that the thermal stability and the char residue of the virgin PP are more than that of filled composites [25]. FWO and KAS degradation kinetic models were used to calculate the activation energies of degradation and they could propose the mechanism of degradation as well.

Esmizadeh et al. studied the degradation kinetics of PP-wood composites using the data from thermogravimetric analysis (TGA) tests employing models such as Kissinger-Akahira-Sunose (KAS), Ozawa-Flynn-Wall (OFW), Friedman, Kissinger and Augis models [26]. They found that for the weight percentage of wood particles, the activation energy showed a significant increase, especially at the initial steps of degradation. Another interesting study from Liang et al. used the kinetic studies of melt blended composites of PP with graphene nanoplatelets [27]. It was found that the mechanism of thermal decomposition a phase boundary controlled reaction (contracting volume) and also the activation energy values increased concerning the increase in filler content and dimension. Additionally, they tried to simulate the process through a decomposition kinetics equation and the experimental values were in good agreement with the simulation results obtained.

Vimalathithan et al. studied the thermal degradation characteristics obtained from TGA measurements of four different PP/clay nanocomposites to different loadings of montmorillonite (MMT), organically modified MMT (OMMT), organically modified hectorite (OMHT), and mica particles [28]. A fixed amount of PP-g-MA was added as the compatibilizer during the compounding. The determined activation energies of the composites showed different trends with MMT and OMHT showing an increase and that with OMMT and mica decreasing concerning change in conversion. The pre-exponential factor, reaction model, and the optimum working temperature of the different PP/clay nanocomposites were also determined and PP/OMMT was found to be the best among the four types studied.

Chrissafis et al. studied the degradation kinetics of isotactic PP with carbon black nanocomposites prepared in a twin screw extruder TGA and DTG [29]. The nanoparticle incorporation improved the onset of degradation of PP. The isoconversional methods of Ozawa, Flynn, and Wall (OFW) and Friedman were used to calculate the activation energies and was proved that nanoparticle incorporation increased it significantly.

In another interesting work melt blending technique was used to prepare halloysite nanotubes (HNTs) incorporated PP/HNTs nanocomposites and their thermal degradation mechanism using TGA measurements in air and inert atmospheres [30]. Activation energies for the composites were calculated using the Friedman model and it increased compared to PP alone. 8 wt% HNT incorporated PP composites were selected as a model compound and simulation curves were developed using different model equations and it was found that the experimental data is similar to the simulated ones.

The preceding discussion highlighted the different reports related to the thermal degradation kinetics of PP and PP-based composites. The composites of PP with TiO₂ have been studied by various research groups, however none of them studied the thermal degradation kinetics. Various investigations reported that TiO₂ can act as thermal stabilizer, antioxidant as well as a reinforcing filler in the polymer matrix. Hence, PP-TiO₂ composite was chosen as the system for the present investiga-

tion. The present study reports the results of the thermal degradation kinetics of the PP reinforced with microparticles of TiO₂ in different loadings. The studies were conducted using a thermogravimetric analyzer at different heating rates in an inert atmosphere. The findings of this study will provide useful insights into the high-temperature applications of PP composites in multifaceted applications. Also, the study pattern will motivate other researchers to find out the exact mechanism of thermal degradation for different polymeric composites.

2. Materials and methods

Polypropylene (random copolymer, R40MLT) with a melt flow index (MFI) value of 40 g/10 min was supplied by NATPET, Yanbu, Saudi Arabia. TiO₂ used in the present investigation was TiONA 244, obtained from Tronox, Yanbu, Saudi Arabia with average particle size of 0.28 μm, specific gravity of 4.1 and oil absorption capacity of 35 g/100 g. The composites of PP and TiO₂ were prepared using a modular co-rotating twin screw extruder with an L/D ratio of 25:1 (Thermo Haake Rheo-drive 16 OS-16 kW). Nine-zone heating was applied during compounding with a temperature profile ranging from 140 °C at the feed zone to 230 °C at the metering zone and the die. The screw speed was maintained at 200 rpm. The strands were cooled in a water bath and subsequently dried and pelletized. The TiO₂ content was varied from 0 wt% to 30 wt% and the corresponding composites were designated as PP, PP-5T, PP-10T, PP-20T, and PP-30T. PP indicates 100 wt% PP and 0 wt% of TiO₂ and PP-30T shows that the TiO₂ is 30 wt% in the composite. Non-isothermal degradation studies were performed with approximately 5 mg sample size using a thermogravimetric analyzer (HITACHI STA7000) at heating rates of 5, 10, 20, and 40 K/min under nitrogen atmospheres from 25 to 600 °C.

2.1. Thermal degradation kinetics; theoretical models

For the thermal degradation of polymeric materials, it is established that the extent of conversion is proportional to the concentration of the reacted material. The rate of conversion is represented by the generalized rate Eq. (1) [31] as follows:

$$\beta \frac{d\alpha}{dT} = K(T)f(\alpha), \quad (1)$$

where $\beta = (dT/dt)$ is the heating rate in K, α is the degree of conversion defined by the following relation:

$$\alpha = \frac{w_i - w}{w - w_f}, \quad (2)$$

where w is the weight of the sample at a given time t , w_i refers to the weight of the sample at the beginning and w_f is the weight of the sample at the end of the experiment of interest. $f(\alpha)$ refers to the function of conversion and $K(T)$ is the temperature-dependent rate of the weight loss during the thermal degradation. $K(T)$ can be related to the activation energy of the degradation reaction by the well-known Arrhenius Eq. (3) [32]:

$$K(T) = A e^{\left(-\frac{E}{RT}\right)}, \quad (3)$$

where E is the activation energy for the thermal degradation reaction, A is the pre-exponential factor and R is the universal gas constant. Substitution of Eq. (3) to Eq. (1) gives the following equation:

$$\beta \frac{d\alpha}{dT} = A e^{\left(-\frac{E}{RT}\right)} f(\alpha). \quad (4)$$

Various differential and integral methods were used by different researchers [33] to obtain the values of activation energy and the pre-exponential factor from the Eq. (4).

2.1.1. Friedman method (FR)

Friedman suggested a differential iso-conversional model [34] based on Eq. (4) and is given as

$$\ln \left(\beta \frac{d\alpha}{dT} \right) = \ln [A f(\alpha)] - \frac{E}{RT}. \quad (5)$$

This equation can be used to find the values of activation energy E for different conversions by plotting $\ln(\beta d\alpha/dT)$ against $1/T$ for constant α values.

2.1.2. Kissinger–Akahira–Sunose (KAS) equation

Akahira et al. [35] proposed an improved method for the determination of activation energy values and is given:

$$\ln \left(\frac{\beta}{T^2} \right) = \text{const.} - \left(\frac{E}{RT} \right). \quad (6)$$

Plots of $\ln(\frac{\beta}{T^2})$ against $(1/T)$ for each conversion α , yields a straight line with a slope directly proportional to activation energy E which is a function of conversion.

2.1.3. Starink method

Starink method [36] uses the above Eq. (6) with some modifications and it takes the following form:

$$\ln \left(\frac{\beta}{T^{1.92}} \right) = \text{const.} - 1.0008 \left(\frac{E}{RT} \right). \quad (7)$$

From the plot of $\ln(\frac{\beta}{T^{1.92}})$ against $(\frac{1}{T})$, the activation energy E can be determined.

2.1.4. Ozawa – Flynn and wall (OFW) method [37]

This method is considered a “model-free” method, derived using integral iso-conversional methods, where the assumption is that the conversion function $f(\alpha)$ does not change with the changes in the heating rate for specific values of α . Also, the temperature (T) corresponding to specific values of α are obtained from TGA experiments at different heating rates of β . The basic equation takes the form of

$$\ln(\beta) = \ln \left[A \frac{f\alpha}{\left(\frac{d\alpha}{dt}\right)} \right] - \left[\frac{E_a}{RT} \right]. \quad (8)$$

Doyle’s linear approximation proposed by Flynn [38,39] can be applied to Eq. (7) and the modified equation takes the following form:

$$\ln(\beta) = \left[\ln \frac{AE}{g(\alpha)R} - 2.315 \right] - \frac{0.457E}{RT}. \quad (9)$$

Plots of $\ln(\beta)$ against $(\frac{1}{T})$ for different conversion α , yield straight lines and the activation energy is obtained from the slopes of these straight lines.

2.1.5. Horowitz and Metzger method

The method suggested by Horowitz and Metzger [40] is an integral method that provides the activation energy for decomposition using the following equation:

$$\ln \left[\ln \frac{1}{(1-\alpha)} \right] = \frac{E\Theta}{RT_{\max}^2}, \quad (10)$$

Where T_{\max} is the maximum decomposition temperature, T is the temperature, Θ is $T - T_{\max}$ and R is the gas constant. By plotting $\ln[\ln \frac{1}{(1-\alpha)}]$ against Θ , E_a can be determined from the slope of the curves.

2.1.6. Coats and Redfern method [41]

This method is considered one of the most successful methods for the calculation of the kinetic parameters of the thermal decomposition of many types of solid materials [42]. Rearrangement and integration of Eq. (5) by this method leads to the following relation:

$$\ln \left[\frac{g(\alpha)}{T^2} \right] = \ln \left(\frac{AR}{\beta E} \right) - \frac{E}{RT}, \quad (11)$$

where, $g(\alpha) = \int_0^\alpha \frac{d\alpha}{f(\alpha)}$.

Table 1
Reaction mechanisms of solid-state processes and their corresponding algebraic expressions for $g(\alpha)$ and $f(\alpha)$ [43].

Symbol	$g(\alpha)$	$f(\alpha)$	Name of the function	Reaction mechanism
1. Chemical process (mechanism non-invoking equations)				
$F_{1/3}$	$1 - (1 - \alpha)^{\frac{2}{3}}$	$(3/2)(1 - \alpha)^{\frac{1}{3}}$	One-third order	Chemical reaction
$F_{3/4}$	$1 - (1 - \alpha)^{\frac{1}{4}}$	$4(1 - \alpha)^{\frac{3}{4}}$	Three-quarters order	Chemical reaction
$F_{3/2}$	$(1 - \alpha)^{-\frac{1}{2}} - 1$	$2(1 - \alpha)^{\frac{3}{2}}$	One-and-a-half order	Chemical reaction
F_2	$(1 - \alpha)^{-1} - 1$	$(1 - \alpha)^2$	Second order	Chemical reaction
F_3	$(1 - \alpha)^{-2} - 1$	$(1/2)(1 - \alpha)^3$	Third order	Chemical reaction
2. Acceleratory rate equations				
$P_{3/2}$	$\alpha^{\frac{3}{2}}$	$(2/3)\alpha^{-\frac{1}{2}}$	Mampel power law	Nucleation
$P_{1/2}$	$\alpha^{\frac{1}{2}}$	$2\alpha^{\frac{3}{2}}$	Mampel power law	Nucleation
$P_{1/3}$	$\alpha^{\frac{1}{3}}$	$3\alpha^{\frac{2}{3}}$	Mampel power law	Nucleation
$P_{1/4}$	$\alpha^{\frac{1}{4}}$	$4\alpha^{\frac{3}{4}}$	Mampel power law	Nucleation
E_1	$\ln \alpha$	α	Exponential law	Nucleation
3. Sigmoidal rate equations (random nucleation and subsequent growth)				
A_1, F_1	$-\ln(1 - \alpha)$	$(1 - \alpha)$	Avrami-Erofeev equation	Assumed random nucleation and its subsequent growth, $n = 1$
$A_{3/2}$	$[-\ln(1 - \alpha)]^{2/3}$	$3/2(1 - \alpha)[- \ln(1 - \alpha)]^{1/3}$	Avrami-Erofeev equation	Assumed random nucleation and its subsequent growth, $n = 1.5$
A_2	$[-\ln(1 - \alpha)]^{1/2}$	$2(1 - \alpha)[- \ln(1 - \alpha)]^{1/2}$	Avrami-Erofeev equation	Assumed random nucleation and its subsequent growth, $n = 2$
A_3	$[-\ln(1 - \alpha)]^{1/3}$	$3(1 - \alpha)[- \ln(1 - \alpha)]^{2/3}$	Avrami-Erofeev equation	Assumed random nucleation and its subsequent growth, $n = 3$
A_4	$[-\ln(1 - \alpha)]^{1/4}$	$4(1 - \alpha)[- \ln(1 - \alpha)]^{3/4}$	Avrami-Erofeev equation	Assumed random nucleation and its subsequent growth, $n = 4$
A_u	$\ln[\alpha/(1 - \alpha)]$	$\alpha(1 - \alpha)$	Prout-Tomkins equation	Branching nuclei
4. Decelerator rate equations				
4.1 Phase boundary reaction				
R_1, F_0, P_1	α	$(1 - \alpha)^0$	Power law	Contracting disk
$R_2, F_{1/2}$	$1 - (1 - \alpha)^{1/2}$	$2(1 - \alpha)^{1/2}$	Power law	Contracting cylinder
$R_3, F_{2/3}$	$1 - (1 - \alpha)^{1/3}$	$3(1 - \alpha)^{2/3}$	Power law	Contracting sphere
4.2 Based on the diffusion mechanism				
D_1	α^2	$1/2\alpha$	Parabola law	One-dimensional diffusion
D_2	$\alpha + (1 - \alpha)\ln(1 - \alpha)$	$-\ln(1 - \alpha)^{-1}$	Valensie equation	Two-dimensional diffusion
D_3	$[1 - (1 - \alpha)^{1/3}]^2$	$3/2(1 - \alpha)^{2/3}[1 - (1 - \alpha)^{1/3}]^{-1}$	Jander equation	Three-dimensional diffusion, spherical symmetry
D_4	$1 - \frac{2\alpha}{3} - (1 - \alpha)^{2/3}$	$3/2[(1 - \alpha)^{-1/3} - 1]^{-1}$	Ginstling-Brounsteinequation	Three-dimensional diffusion, cylindrical symmetry
D_5	$[(1 - \alpha)^{-1/3} - 1]^2$	$3/2(1 - \alpha)^{4/3}[(1 - \alpha)^{-1/3} - 1]^{-1}$	Zhuravlev, Lesokin, Tempelman equation	Three-dimensional diffusion
D_6	$[(1 + \alpha)^{1/3} - 1]$	$3/2(1 + \alpha)^{2/3}[(1 + \alpha)^{1/3} - 1]^{-1}$	anti-Jander equation	Three-dimensional diffusion
D_7	$1 + \frac{2\alpha}{3} - (1 + \alpha)^{2/3}$	$3/2[(1 + \alpha)^{-1/3} - 1]^{-1}$	anti-Ginstling-Brounsteinequation	Three-dimensional diffusion
D_8	$[(1 + \alpha)^{-1/3} - 1]$	$3/2(1 + \alpha)^{4/3}[(1 + \alpha)^{-1/3} - 1]^{-1}$	anti-Zhuravlev, Lesokin, Tempelman equation	Three-dimensional diffusion
5. Other kinetic equations with the unjustified mechanism				
G_1	$1 - (1 - \alpha)^2$	$1/2(1 - \alpha)$		
G_2	$1 - (1 - \alpha)^3$	$1/3(1 - \alpha)^2$		
G_3	$1 - (1 - \alpha)^4$	$1/4(1 - \alpha)^3$		
G_4	$[-\ln(1 - \alpha)]^2$	$1/2(1 - \alpha)[- \ln(1 - \alpha)]^{-1}$		
G_5	$[-\ln(1 - \alpha)]^3$	$1/3(1 - \alpha)[- \ln(1 - \alpha)]^{-2}$		
G_6	$[-\ln(1 - \alpha)]^4$	$1/4(1 - \alpha)[- \ln(1 - \alpha)]^{-3}$		
G_7	$[1 - (1 - \alpha)^{1/2}]^{1/2}$	$4\{(1 - \alpha)[1 - (1 - \alpha)^{1/2}]\}^{1/2}$		
G_8	$[1 - (1 - \alpha)^{1/3}]^{1/2}$	$6(1 - \alpha)^{2/3}[1 - (1 - \alpha)^{1/3}]^{1/2}$		

Plot of $\ln[\frac{g(\alpha)}{T^2}]$ versus $\frac{1}{T}$ for a selected heating rate β for an appropriate degradation function $f(\alpha)$ results in the determination of apparent activation energy E_a and the Arrhenius pre-exponential factor A . The most widely used reaction mechanism for solid-state processes and the corresponding algebraic expressions for $g(\alpha)$ and $f(\alpha)$ are given in Table 1 [43].

2.1.7. Criado method [44]

In this method, the Eqs. (4)–(11) are combined to arrive at the following equation:

$$\frac{Z(\alpha)}{Z(0.5)} = \frac{f(\alpha)g(\alpha)}{f(0.5)g(0.5)} = \left(\frac{T_\alpha}{T_{0.5}}\right)^2 \frac{\left(\frac{d\alpha}{dt}\right)_\alpha}{\left(\frac{d\alpha}{dt}\right)_{0.5}} \tag{12}$$

Where 0.5 refers to the conversion corresponding to $\alpha = 0.5$. When appropriate expressions for $g(\alpha)$ and $f(\alpha)$ from Table 1 are used, the left-

hand side of the Eq. (12) closely matches the experimental data given on the right-hand side of the same equation.

3. Results and discussion

The TG and DTG curves for PP at a heating rate of 5 K/min are shown in Fig. 1(a) and the representative thermograms of PP at four different heating rates (5, 10, 20, and 40 K/min) are given in Fig. 1(b). The DTG peak represents the maximum degradation temperature of that sample and it slightly increases with an increase in the heating rate, due to the shorter time available to arrive at a particular higher temperature during the experiment. More details pertaining to the TG and DTG curves for the composites are given in the supplementary file [Figs. S1(a)–(e)]. The thermal degradation experiments at various heating rates provide valuable insights into the mechanism of this process and the various mathematical models based on the Arrhenius equation can be utilized for this purpose. Carefully designed thermal degradation experiments

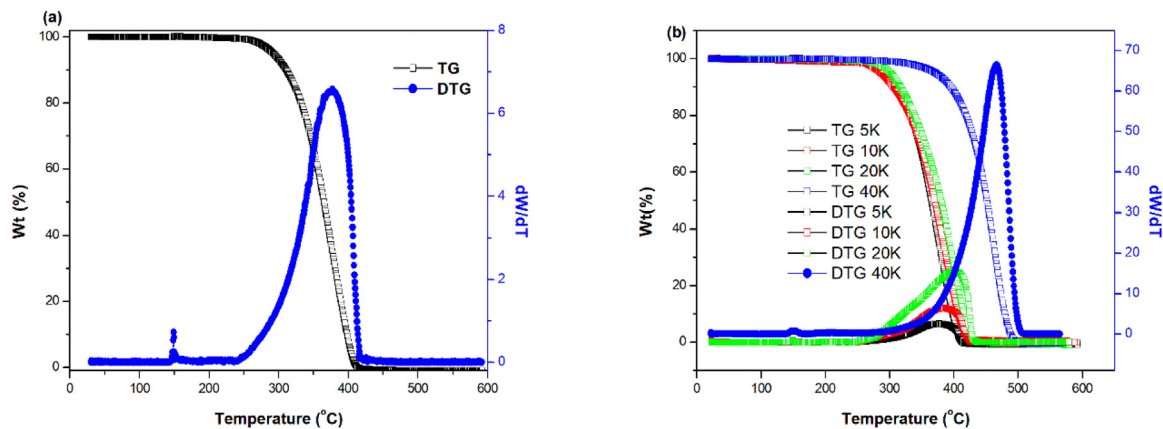


Fig. 1. (a) TG and DTG curves for PP (heating rate 5 K/min) and (b) TG and DTG curves for PP at various heating rates.

Table 2

Activation energy E_a and regression coefficient values for PP and the composites from Friedman model equation.

Conversion (α)	PP		PP-5T		PP-10T		PP-20T		PP-30T	
	E_a (kJ mol ⁻¹)	R^2	E_a (kJ mol ⁻¹)	R^2	E_a (kJ mol ⁻¹)	R^2	E_a (kJ mol ⁻¹)	R^2	E_a (kJ mol ⁻¹)	R^2
0.1	58	0.720	77	0.920	69	0.805	79	0.979	83	0.984
0.2	64	0.792	100	0.950	81	0.857	83	0.973	93	0.994
0.3	72	0.838	112	0.966	89	0.899	86	0.991	104	0.991
0.4	77	0.860	118	0.962	94	0.933	92	0.987	120	0.993
0.5	88	0.858	121	0.979	100	0.937	96	0.979	129	0.986
0.6	89	0.861	113	0.960	94	0.953	95	0.976	134	0.966
0.7	100	0.864	99	0.955	90	0.915	94	0.974	131	0.940
0.8	95	0.811	94	0.964	67	0.865	79	0.931	115	0.894
0.9	83	0.693	84	0.965	71	0.846	78	0.976	106	0.900
Average	82	0.811	102	0.958	84	0.890	87	0.974	113	0.961

and their analysis can help in predicting the mechanism of degradation beyond the experimental temperature range [45].

3.1. Friedman model

Friedman model follows the iso-conversional method to obtain the accurate values of kinetic parameters of the thermal degradation process [46]. Plots of $\ln(\beta \frac{d\alpha}{dT})$ against $\frac{1}{T}$ for α values ranging from 0.1 to 0.9 for PP and its composites with TiO₂ are given in Figs. 2(a)–(e). The activation energy E_a for these samples are given in Table 2. For all the samples, the E_a value gradually increases as the conversion percentage (α) increases and reach a maximum value near $\alpha = 0.5$. As the temperature increases, the thermal degradation process proceeds through three different stages viz initiation, propagation and termination [47]. During the middle stages of the degradation process ($\alpha = 0.2$ to 0.5), tertiary radicals are formed and this results in an appreciable increase in the E_a values as well as a change in the degradation mechanism at this stage [48]. The activation energy (E_a) for the thermal degradation of PP obtained as an average from those at various conversions is 82 kJ mol⁻¹, which is similar to the value reported by Paik et al. [49]. The value increased to 102 kJ mol⁻¹ with the incorporation of 5 wt% of TiO₂ in PP. The E_a values decreased to 84 and 87 kJ mol⁻¹ respectively, with further increase in the TiO₂ content to 10 wt% and 20 wt% in the PP matrix. However, the E_a value reached a maximum of 113 kJ mol⁻¹ with a further increase in TiO₂ to 30 wt%. This indicates that more energy is consumed for thermal degradation of the composites when TiO₂ levels in the composites reach 5 wt% and 30 wt%.

3.2. Kissinger–Akahira–Sunose (KAS) equation

Plots of $\ln(\frac{\beta}{T^2})$ against $(\frac{1}{T})$ for PP and its composites with TiO₂ for each conversion α are given in Figs. 3(a)–(e). The activation energy E_a obtained from these plots for various conversion stages (α) is given in

Table 3. The activation energy (E_a) for thermal degradation of PP obtained as an average of various conversion stages from 0.1 to 0.9 is 61 kJ mol⁻¹, which is slightly lower than that obtained by the Friedman model. The value increased to 85 kJ mol⁻¹ with the incorporation of 5 wt% of TiO₂ into the base matrix. The E_a values decreased to 77 and 81 kJ mol⁻¹ respectively, with further increase in the TiO₂ content to 10 wt% and 20 wt% in the PP matrix. However, the E_a value reached a maximum of 100 kJ mol⁻¹ with a further increase in TiO₂ to 30 wt%.

3.3. Starink method

Plots of $\ln(\frac{\beta}{T^{1.92}})$ against $(\frac{1}{T})$ for PP and the composites are shown in Figs. 4(a)–(e). The activation energy E_a obtained from these plots for various conversion stages (α) is given in Table 4. The activation energy (E_a) for thermal degradation of PP obtained as an average of conversion stages (α) from 0.1 to 0.9 is 62 kJ mol⁻¹, which is very similar to the value obtained from the KAS model equation. The value increased to 85 kJ mol⁻¹ with the incorporation of 5 wt% of TiO₂ into the base matrix. The E_a values decreased to 78 and 82 kJ mol⁻¹ respectively, with further increase in the TiO₂ content to 10 wt% and 20 wt% in the PP matrix. However, the E_a value reached a maximum of 102 kJ mol⁻¹ with a further increase in TiO₂ to 30 wt%.

3.4. Ozawa – Flynn and Wall (OFW) method

Plots of $\ln(\beta)$ against $(\frac{1}{T})$ for PP and the composites are given in Figs. 5(a)–(e) respectively. The activation energy E_a obtained from these plots for various conversion stages (α) is given in Table 5. The activation energy (E_a) for thermal degradation of PP obtained as an average of conversion stages (α) from 0.1 to 0.9 is 159 kJ mol⁻¹, which is very similar to the value reported by Galiwango et al. [50]. The value increased to 211 kJ mol⁻¹ with the incorporation of 5 wt% of TiO₂ into the base matrix. The E_a values decreased to 194 and 201 kJ mol⁻¹ respectively,

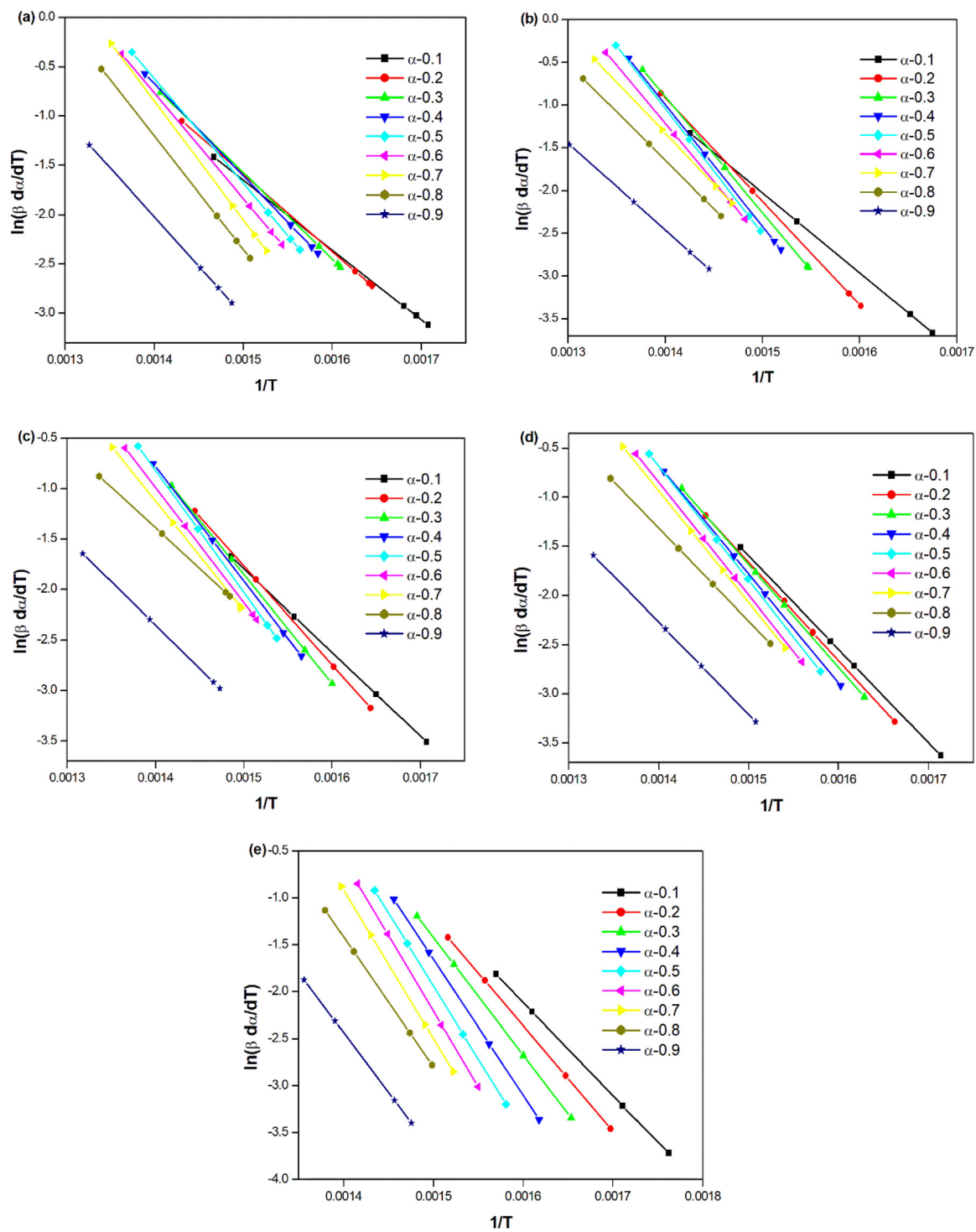


Fig. 2. Friedman model plots for (a) PP, (b) PP-5T, (c) PP-10T, (d) PP-20T, and (e) PP-30T.

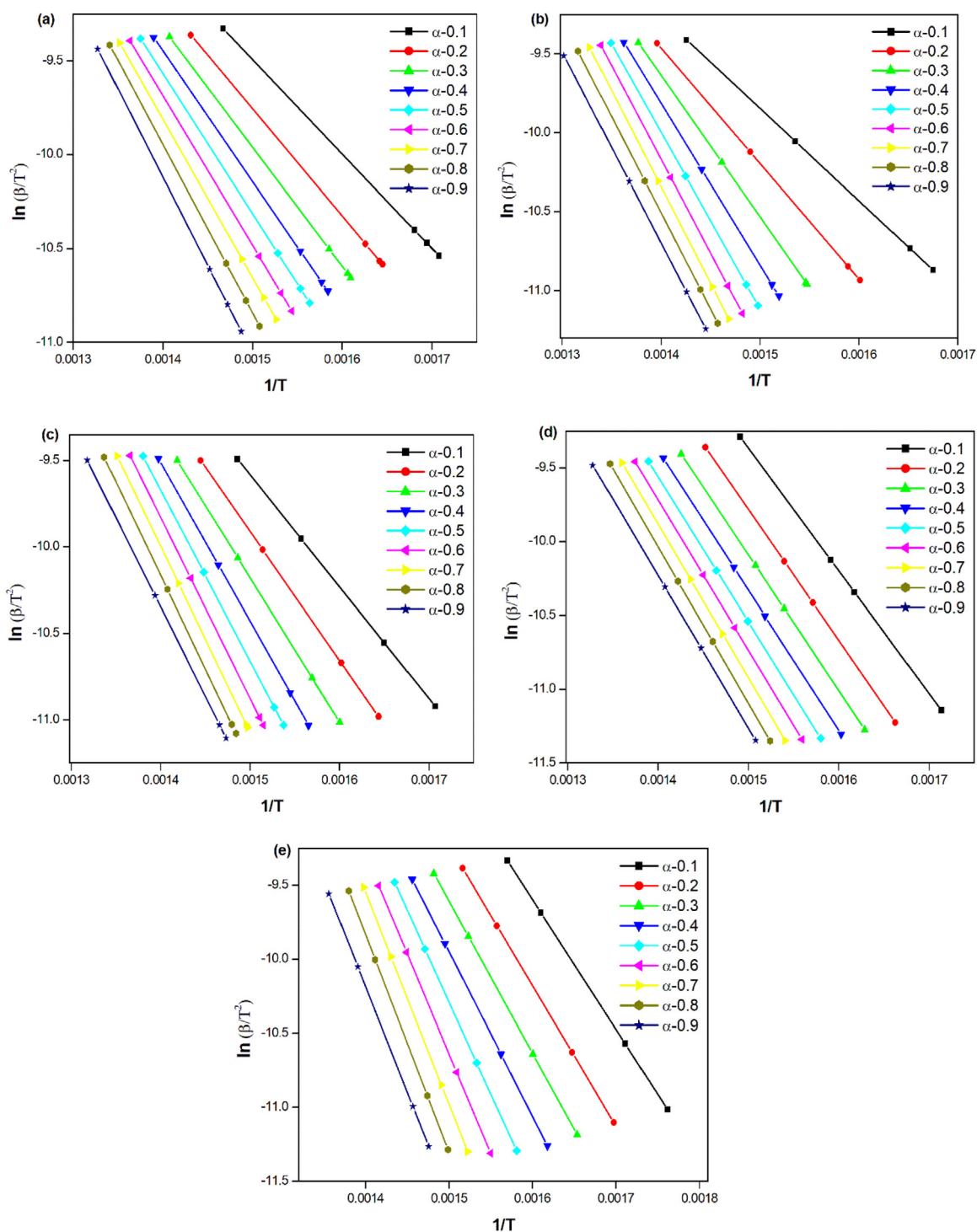


Fig. 3. KAS model plots for (a) PP, (b) PP-5T, (c) PP-10T, (d) PP-20T and (e) PP-30T.

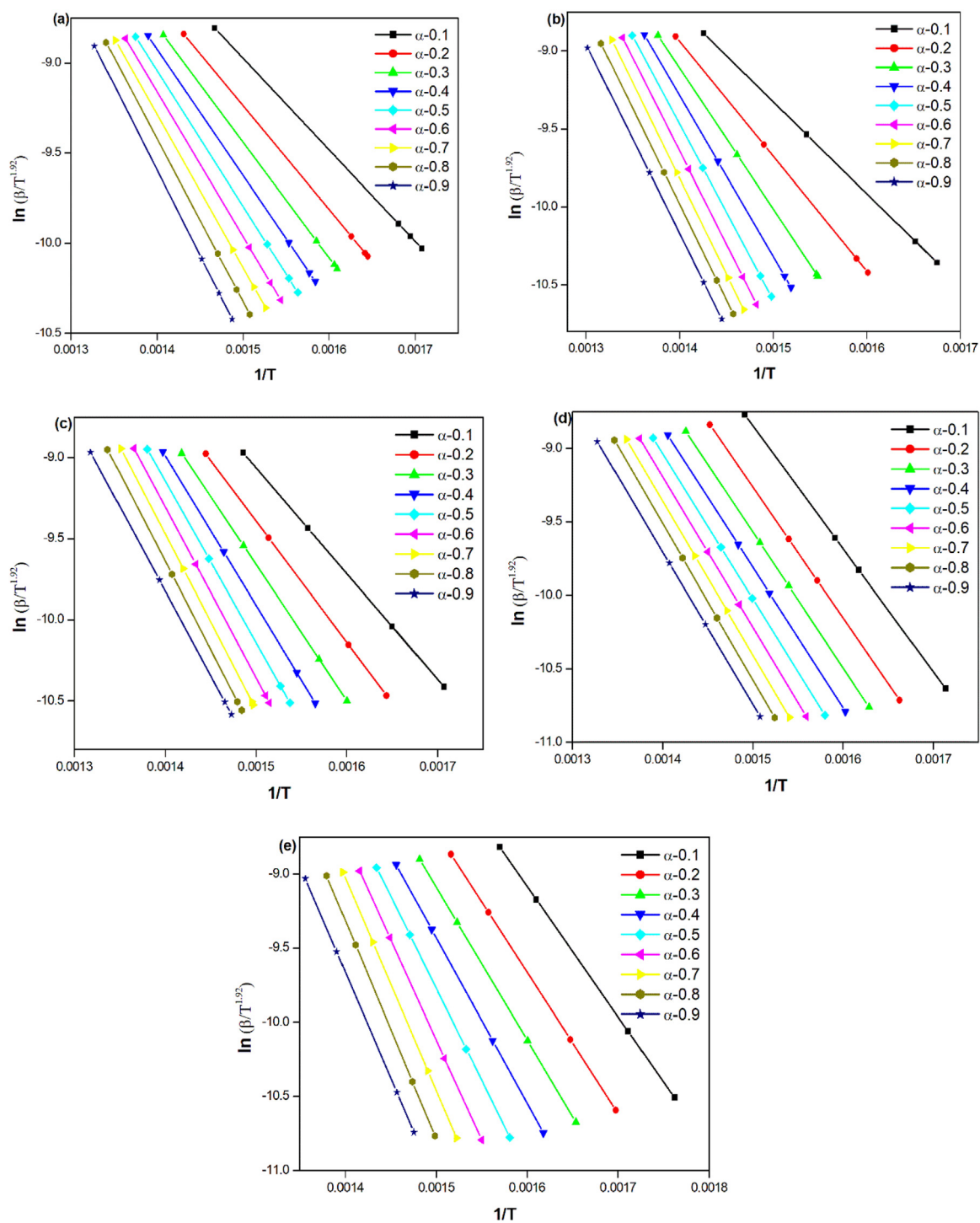


Fig. 4. Starink model plots for (a) PP, (b) PP-5T, (c) PP-10T, (d) PP-20T, and (e) PP-30T.

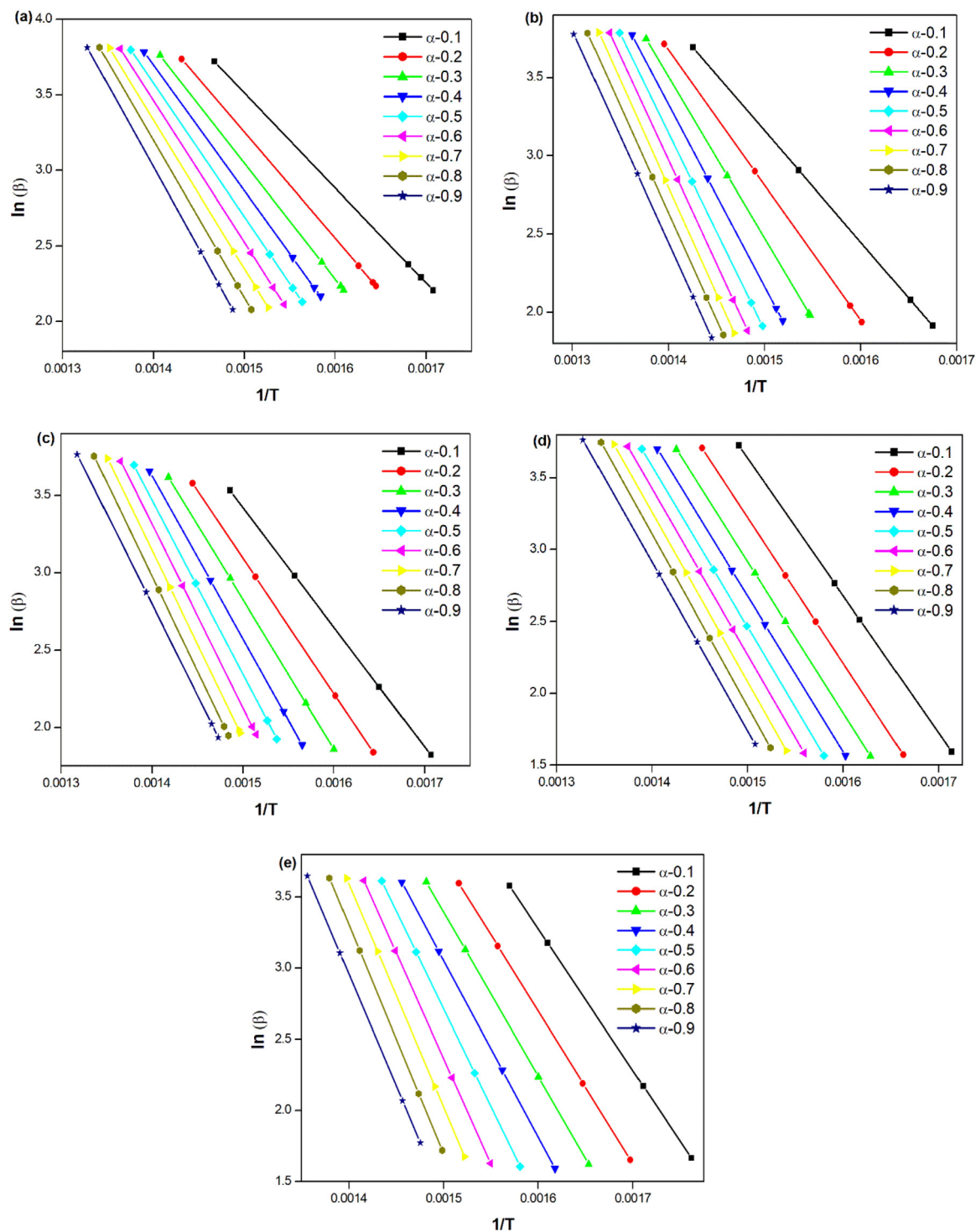


Fig. 5. O-F-W model plots for (a) PP, (b) PP-5T, (c) PP-10T, (d) PP-20T and (e) PP-30T.

Table 3Activation energy E_a and regression coefficient values from the KAS model equation for PP and the composites.

Conversion (α)	PP		PP-5T		PP-10T		PP-20T		PP-30T	
	E_a (kJ mol ⁻¹)	R^2	E_a (kJ mol ⁻¹)	R^2	E_a (kJ mol ⁻¹)	R^2	E_a (kJ mol ⁻¹)	R^2	E_a (kJ mol ⁻¹)	R^2
0.1	42	0.534	49	0.782	54	0.640	69	0.946	73	0.965
0.2	47	0.561	61	0.817	62	0.696	74	0.962	79	0.974
0.3	53	0.609	75	0.856	69	0.739	76	0.964	85	0.985
0.4	58	0.651	85	0.887	76	0.783	79	0.971	92	0.988
0.5	62	0.685	93	0.904	82	0.826	82	0.974	103	0.989
0.6	66	0.701	99	0.919	87	0.853	85	0.977	112	0.987
0.7	70	0.719	101	0.926	89	0.877	87	0.978	119	0.980
0.8	75	0.729	101	0.933	90	0.887	88	0.982	122	0.967
0.9	78	0.728	100	0.941	86	0.891	86	0.979	119	0.952
Average	61	0.657	85	0.885	77	0.799	81	0.970	100	0.976

Table 4Activation energy E_a and regression coefficient values from Starink model equation for PP and the composites.

Conversion (α)	PP		PP-5T		PP-10T		PP-20T		PP-30T	
	E_a (kJ mol ⁻¹)	R^2	E_a (kJ mol ⁻¹)	R^2	E_a (kJ mol ⁻¹)	R^2	E_a (kJ mol ⁻¹)	R^2	E_a (kJ mol ⁻¹)	R^2
0.1	43	0.540	49	0.785	55	0.644	70	0.947	74	0.965
0.2	48	0.565	62	0.819	63	0.698	75	0.962	80	0.975
0.3	54	0.613	76	0.857	70	0.741	77	0.964	87	0.985
0.4	59	0.654	86	0.888	77	0.785	80	0.972	94	0.988
0.5	63	0.688	94	0.905	83	0.828	83	0.974	104	0.989
0.6	67	0.704	100	0.920	88	0.854	86	0.977	113	0.987
0.7	71	0.722	103	0.927	90	0.878	88	0.978	120	0.980
0.8	76	0.732	103	0.933	91	0.888	89	0.982	124	0.968
0.9	79	0.731	102	0.941	87	0.892	87	0.979	120	0.953
Average	62	0.661	86	0.886	78	0.801	82	0.971	102	0.977

Table 5Activation energy E_a and regression coefficient values from O-F-W model equation for PP and the composites.

Conversion (α)	PP		PP-5T		PP-10T		PP-20T		PP-30T	
	E_a (kJ mol ⁻¹)	R^2	E_a (kJ mol ⁻¹)	R^2	E_a (kJ mol ⁻¹)	R^2	E_a (kJ mol ⁻¹)	R^2	E_a (kJ mol ⁻¹)	R^2
0.1	114	0.643	130	0.842	141	0.716	174	0.959	181	0.972
0.2	128	0.659	157	0.862	159	0.758	184	0.970	195	0.980
0.3	140	0.695	188	0.887	176	0.791	191	0.972	210	0.988
0.4	151	0.727	211	0.910	191	0.826	197	0.978	226	0.991
0.5	161	0.753	229	0.923	205	0.860	203	0.980	249	0.991
0.6	170	0.765	242	0.935	215	0.881	210	0.982	270	0.989
0.7	179	0.778	248	0.940	221	0.901	215	0.983	285	0.983
0.8	189	0.784	248	0.946	223	0.910	218	0.986	293	0.973
0.9	197	0.781	246	0.953	214	0.914	214	0.984	286	0.960
Average	159	0.732	211	0.911	194	0.840	201	0.977	244	0.981

with further increase in the TiO₂ content to 10 wt% and 20 wt% in the PP matrix. However, the E_a value reached a maximum of 244 kJ mol⁻¹ with a further increase in TiO₂ to 30 wt%.

All the results depicted in Tables 2–5 follow a similar pattern. The activation energy value of virgin PP is less than that of all the filled composites. When 5 wt% of TiO₂ is added, it seems that the particles are well dispersed in the matrix enhancing the filler-matrix interactions. The strong filler-matrix interaction can restrict the mobility of the polymer chains, which can lead to a more energy-intensive process during the thermal degradation [51]. Naturally, the activation energy value will increase compared with the virgin matrix. Another factor is the increased crystallinity of PP due to the nucleating effect of the added filler. The ordered structure formed due to the increased crystallinity of the matrix needs more energy to break down the chains thereby leading to enhanced activation energy values [52–54].

Activation energy values were lower for the 10 wt% and 20 wt% addition of filler to PP as per the different kinetic models. Several factors might have contributed to this behavior. As the filler content is increased the chances of filler-filler interaction increases thereby leading to particle agglomeration in the matrix. The effective surface area of the filler is reduced due to the particle agglomeration which decreases the interfacial interactions between the polymer and filler which im-

parts fewer restrictions on the mobility of the polymer chains [55]. Another factor is the increase in thermal conductivity of the composites due to the higher loading of the fillers which facilitate the effective heat transfer during degradation [56]. The plasticizing effect of the fillers at these loadings may also contribute to the reduction of the activation energy [57].

The increase in activation energy at 30 wt% loading can be related to many factors. At this high loading of the filler, TiO₂ particles are behaving like real reinforcement for the PP matrix. This reinforcement action increases the resistance to thermal degradation which thereby increases the activation energy. Higher filler loading also increases the tortuous path for the release of the volatile degradation products. Thus, it delays the degradation process which naturally increases the activation energy values. Another important factor is the ability of the filler to form a continuous network in the polymer matrix which will act as a barrier to the transfer of heat and mass. This barrier effect will delay the thermal degradation process which leads to higher activation energy values [57,58].

The Friedman model presented above follows a differential method, whereas, O-F-W, KAS, and Starink models are integral methods to obtain activation energy from iso-conversional plots. Among these three integral methods, O-F-W method utilizes an approximation for the tem-

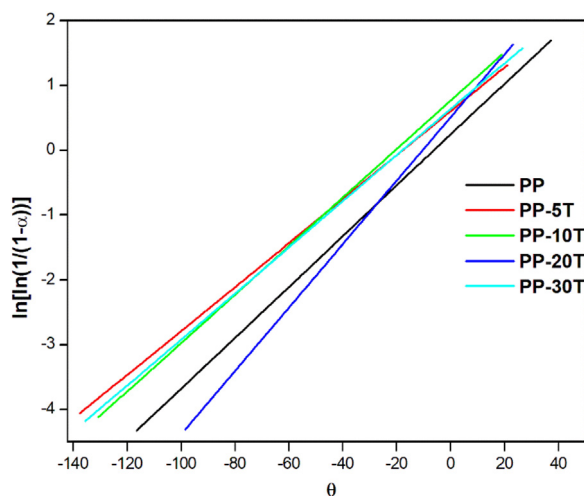


Fig. 6. Horowitz and Metzger method plots for PP and the composites.

Table 6

Activation energy E_a and regression coefficient values from Horowitz and Metzger model equation for PP and the composites.

Sample	E_a (kJ mol ⁻¹)	R^2
PP	48	0.953
PP-5T	50	0.935
PP-10T	50	0.945
PP-20T	68	0.957
PP-30T	78	0.942

perature integral which is less accurate than the approximation used by other methods, which leads to higher values of E_a [59]. However, to understand the exact mechanism of thermal degradation, other models are to be employed.

3.5. Horowitz and Metzger method

Unlike the multiple heating rate experiments and the corresponding mathematical models mentioned above, Horowitz and Metzger's method can expound the activation energy for the thermal degradation of samples from the experiment carried out at one constant heating rate [60]. Plots of $\ln[\ln \frac{1}{(1-\alpha)}]$ against Θ for PP and the composites for the heating rate of 10 K/min are shown in Fig. 6. The activation energy E_a obtained from these plots are given in Table 6. The E_a value for PP from this method was 48 kJ mol⁻¹ and the values gradually increased with an increase in TiO₂ content in the composites and reached a maximum of 78 kJ mol⁻¹ for the composite that contain 30 wt% of TiO₂.

The reason for the increasing trend of activation energy according to the Horowitz and Metzger method can be correlated to the fact that it mainly focuses on the initial stages of degradation of the polymer matrix or the composites [61]. At this range, the barrier effect and restricted chain mobility are very important. The filler may act as a protective layer over the surface of the polymer matrix which slows down the degradation process and increases the activation energy for filled composites [62,63]. This could explain why it shows a consistent increasing trend, whereas other methods (e.g., Kissinger or Flynn-Wall-Ozawa) might reflect different aspects of the degradation process, such as the influence of filler agglomeration or thermal conductivity.

3.6. Coats and Redfern method

The model equation of the Coats and Redfern method is successfully employed in studying the degradation kinetics of various types of solid substances as it provides information about the probable reaction mechanism in addition to the activation energy values of such thermal

degradation process [64]. Plot of $\ln[\frac{g(\alpha)}{T^2}]$ versus $\frac{1}{T}$ for a heating rate 10 K/min for PP and various composites were made by selecting all the 35 algebraic expressions for the degradation function $g(\alpha)$ given in Table 1. The expressions that result in anomalous values for the kinetic parameters compared with those obtained from other model equations and also those expressions, which produce poor correlation coefficients were excluded. From the remaining expressions, the ones that yield the maximum values (near 1) for the correlation coefficients were selected for elucidating the kinetic parameters as well as the mechanism of thermal degradation of the samples. The selected models based on these criteria and the corresponding kinetic parameters and the degradation mechanisms are given in Table 7. From the table, it can be seen that the equations designated as $F_{3/4}$, R_2 , R_3 , D_3 , and D_4 fit well for the thermal degradation of PP with a correlation coefficient of 0.999. Among these, R_3 is chosen as the mechanism for PP as the activation energy value obtained by using this expression is 86 kJ mol⁻¹, which is very close to that obtained from the iso-conversional Friedman model equation described above. Such a comparison and subsequent selection of the preferred reaction model as R_3 for thermal degradation of PP was reported by Aboulkas et al. [65]. The expression designated as R_2 fits well for the composites with the activation energy values close to those obtained from other model equations. R_3 represents the power law model equation with the thermal degradation mechanism corresponding to the contracting sphere and R_2 represents the contracting cylinder mechanism. With the incorporation of TiO₂, the thermal degradation mechanism of PP changed from the contracting sphere model to the contracting cylinder. The R_3 model assumes that the reaction occurs at the surface of the spherical particle. The reaction front moves inwards as the degradation proceeds. Usually, such a mechanism is shown by the homogeneous materials or systems where the degradation happens uniformly throughout the bulk. When the model is according to R_2 , which is normally associated with systems having anisotropic structures or interfaces in it, the reaction happens on the surface of cylindrical particles and radial inward movement of the reaction front is visible [66,67]. The contracting cylinder model usually shows a different energy profile compared to the contracting sphere model, reflecting the altered degradation pathway [68]. A similar change in mechanism from R_3 to R_2 was reported by Navid et al. [69] in PP/Poly(lactic acid)/clay nanocomposites, where the neat PP followed the contracting sphere mechanism and the rest of the composites shifted to the contracting cylinder mechanism.

The change from the contracting sphere model to the contracting cylinder model due to the TiO₂ filling in PP can be correlated to multiple factors such as the introduction of interfaces and anisotropic heat transfer caused by TiO₂ particles, the barrier effect of TiO₂ which alters the degradation pathway and the changes in polymer morphology such as increased crystallinity and filler agglomeration. These factors collectively influence the degradation mechanism, leading to the observed change in the kinetic model. The Coats-Redfern method is sensitive to these changes and can accurately reflect the altered degradation behavior [70].

3.7. Criado method

Based on the ICTAC recommendations, the Criado model fitting method along with the Coats and Redfern method, is highly preferred for the determination of kinetics parameters as well as the thermal degradation mechanism of PP [48]. For the heating rate of 10 K/min, the appropriate expressions for $g(\alpha)$ and $f(\alpha)$ from Table 1 were substituted in Eq. (12) for the Criado model. Theoretical master curves were plotted based on these expressions and compared with the experimental data. Based on the same criteria mentioned above for the Coats and Redfern method, the expressions that do not fit well with the experimental data were excluded and the remaining expressions were compared with those of the experimental values and presented in Fig. 7. From Fig. 7(a), it can be seen that the expression designated as A_2 fits well with the experimental data for the thermal degradation of PP, whereas the expression

Table 7
The kinetic parameters and the reaction mechanism obtained by applying Coats and Redfern method.

Sample	Symbol	$g(\alpha)$	E_a (kJ mol ⁻¹)	R^2	Name of the function	Reaction mechanism
PP	$F_{3/4}$	$1 - (1 - \alpha)^{1/2}$	89	0.999	Three-quarters order	Chemical reaction
PP-5T			80	0.977		
PP-10T			83	0.993		
PP-20T			124	0.995		
PP-30T			78	0.993		
PP	$P_{3/2}$	$\alpha^{3/2}$	107	0.989	Mampel power law	Nucleation
PP-5T			98	0.998		
PP-10T			100	0.994		
PP-20T			149	0.996		
PP-30T			95	0.993		
PP	A_2	$[-\ln(1 - \alpha)]^{1/2}$	43	0.996	Avrami-Erofeev equation	Assumed random nucleation and its subsequent growth, $n = 2$
PP-5T			38	0.953		
PP-10T			40	0.983		
PP-20T			62	0.988		
PP-30T			37	0.983		
PP	R_1, F_0, P_1	α	68	0.988	Power law	Contracting disk
PP-5T			61	0.998		
PP-10T			63	0.993		
PP-20T			96	0.996		
PP-30T			60	0.992		
PP	$R_2, F_{1/2}$	$1 - (1 - \alpha)^{1/2}$	81	0.999	Power law	Contracting cylinder
PP-5T			73	0.987		
PP-10T			76	0.997		
PP-20T			114	0.999		
PP-30T			71	0.997		
PP	$R_3, F_{2/3}$	$1 - (1 - \alpha)^{1/3}$	86	0.999	Power law	Contracting sphere
PP-5T			77	0.981		
PP-10T			80	0.995		
PP-20T			121	0.997		
PP-30T			76	0.995		
PP	D_1	α^2	146	0.990	Parabola law	One-dimensional diffusion
PP-5T			134	0.998		
PP-10T			137	0.995		
PP-20T			203	0.996		
PP-30T			130	0.994		
PP	D_2	$\alpha + (1 - \alpha)\ln(1 - \alpha)$	162	0.997	Valensie equation	Two-dimensional diffusion
PP-5T			148	0.994		
PP-10T			152	0.998		
PP-20T			225	0.999		
PP-30T			144	0.997		
PP	D_3	$[1 - (1 - \alpha)^{1/3}]^2$	182	0.999	Jander equation	Three-dimensional diffusion, spherical symmetry
PP-5T			165	0.983		
PP-10T			171	0.996		
PP-20T			252	0.997		
PP-30T			161	0.995		
PP	D_4	$1 - \frac{2\alpha}{3} - (1 - \alpha)^{2/3}$	167	0.999	Ginstling-Brounstein equation	Three-dimensional diffusion, cylindrical symmetry
PP-5T			154	0.991		
PP-10T			158	0.998		
PP-20T			233	0.999		
PP-30T			150	0.997		
PP	D_6	$[(1 + \alpha)^{1/3} - 1]^2$	131	0.984	anti-Jander equation	Three-dimensional diffusion
PP-5T			121	0.998		
PP-10T			124	0.990		
PP-20T			183	0.993		
PP-30T			117	0.989		
PP	D_7	$1 + \frac{2\alpha}{3} - (1 + \alpha)^{2/3}$	136	0.986	anti-Ginstling-Brounstein equation	Three-dimensional diffusion
PP-5T			125	0.998		
PP-10T			128	0.992		
PP-20T			190	0.994		
PP-30T			121	0.991		

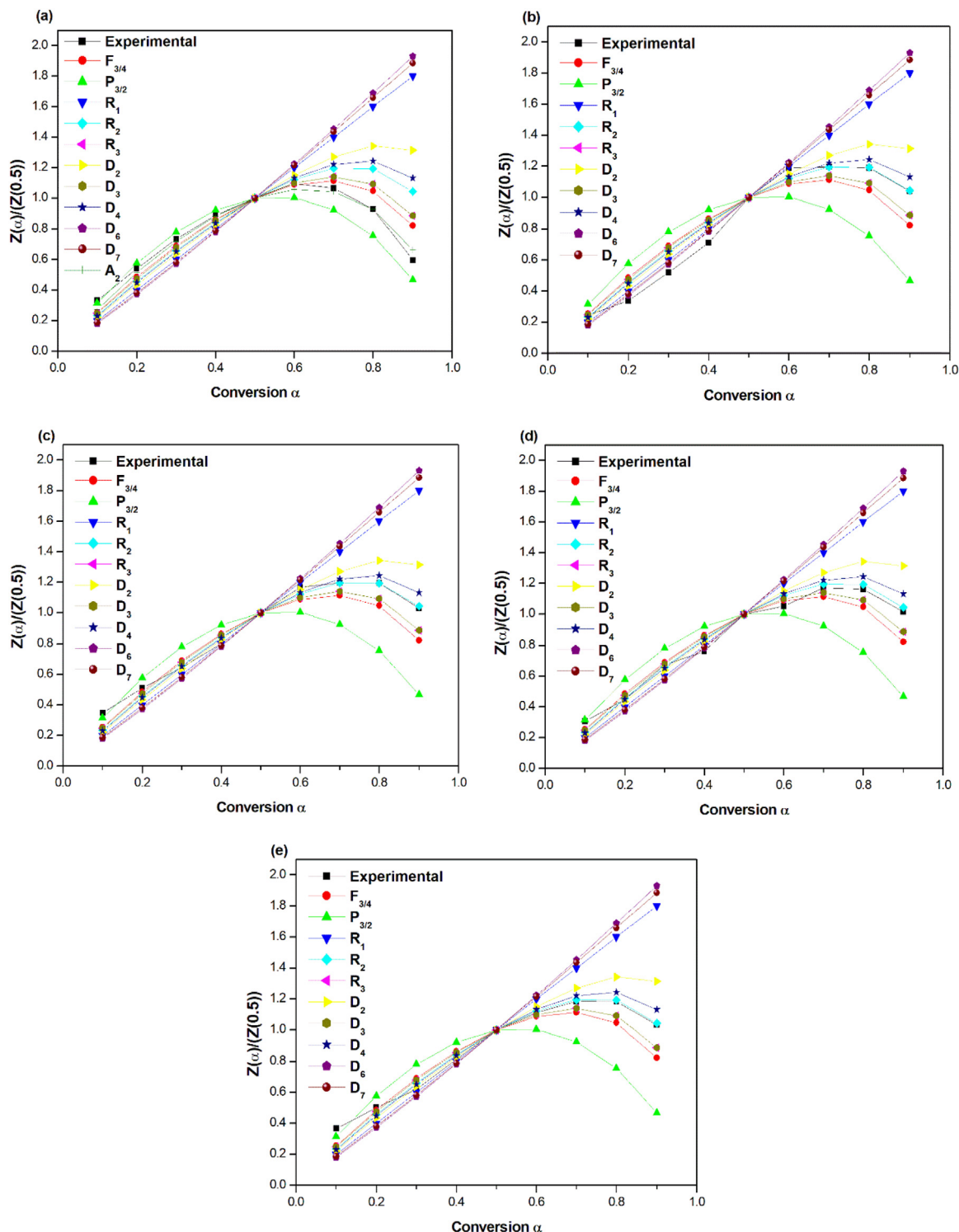


Fig. 7. Criado model plots for (a) PP, (b) PP-5T, (c) PP-10T, (d) PP-20T and (e) PP-30T.

R_2 closely matches all the composites that contain TiO_2 (Figs. 7(b)–(e)). A_2 stands for the Avrami–Erofeev equation, which assumes the mechanism of random nucleation and its subsequent growth. The power law-contracting cylinder mechanism (R_2) represents the degradation mechanism of all the composites that contain TiO_2 . The shift from the Avrami–Erofeev (A_2) mechanism to the power law-contracting cylinder (R_2) mechanism in the thermal degradation of PP with TiO_2 incorporation can be due to factors such as the introduction of interfaces and anisotropic heat transfer caused by TiO_2 particles, the barrier effect of TiO_2 , which alters the degradation pathway and the changes in poly-

mer morphology, such as increased crystallinity and filler agglomeration. The change in the kinetic model is attributed to the influence of multiple factors affecting the degradation mechanism, as described above. The Criado model accounts for these variations, demonstrating alternative degradation behavior for the composites [71–73].

4. Conclusions

The thermal degradation kinetics of PP composites filled with TiO_2 were investigated using various kinetic models, including the Horowitz-

Metzger method, Coats-Redfern method, and Criado model. The results revealed significant changes in the degradation mechanism and activation energy (E_a) with increasing TiO₂ loading, highlighting the complex interplay between the polymer matrix and the filler. The key findings and conclusions are summarized below:

Activation energy trends

The Friedman, O-F-W, KAS, and Starink models resulted in a higher activation energy for the filled systems compared with that of virgin PP, whereas, the composites that contain 5 wt% and 30 wt% of TiO₂ exhibited highest values among the composites. The Horowitz-Metzger method showed an increasing trend in activation energy with increasing TiO₂ loading. This increase can be attributed to the barrier effect of TiO₂ particles, which restricts heat and mass transfer during degradation, restricted chain mobility due to the enhanced interfacial interactions between the polymer and filler, and the formation of the increased tortuosity at higher filler loading.

Degradation mechanism shifts

The Coats-Redfern method indicated a shift in the degradation mechanism from the contracting sphere model (R_3) for pure PP to the contracting cylinder model (R_2) for TiO₂-filled composites. The Criado model further confirmed this shift, showing a transition from the Avrami-Erofeev (A_2) mechanism (random nucleation and growth) for pure PP to the power law-contracting cylinder (R_2) mechanism for TiO₂-filled composites.

Role of TiO₂ in thermal degradation

At low filler loadings (e.g., 5 wt%), TiO₂ improves thermal stability by enhancing interfacial interactions and acts as a nucleating agent, leading to increased activation energy. At intermediate loadings (e.g., 10–20 wt%), filler agglomeration and reduced interfacial interactions can lower activation energy temporarily, but the barrier effect and tortuosity still play a significant role. At high loadings (e.g., 30 wt%), the formation of a continuous filler network dominates, significantly increasing activation energy and altering the degradation mechanism to a more cylindrical pathway.

The kinetic models used in this study (Horowitz-Metzger, Coats-Redfern, and Criado) provide complementary insights into the degradation behavior, confirming the significant role of TiO₂ in altering the thermal degradation kinetics of PP. The findings suggest that TiO₂ can be used as an effective filler to improve the thermal stability of PP composites, especially at higher loadings. The shift in degradation mechanisms highlights the importance of filler dispersion and interfacial interactions in designing thermally stable polymer composites. These results provide valuable insights for applications requiring enhanced thermal performance, such as automotive components, electrical appliances and construction materials.

Declaration of Competing Interest

The authors declare that they have no known financial interests or personal relationships that could have appeared to influence the work reported in this paper.

CRedit authorship contribution statement

Krishna Prasad Rajan: Writing – review & editing, Writing – original draft, Visualization, Validation, Supervision, Software, Resources, Methodology, Investigation, Formal analysis, Data curation, Conceptualization. **Mohammed Rafic:** Validation, Supervision, Software, Resources, Methodology, Investigation. **Selvin P. Thomas:** Writing – review & editing, Writing – original draft, Validation, Supervision, Resources, Methodology, Investigation, Conceptualization.

Supplementary materials

Supplementary material associated with this article can be found, in the online version, at [doi:10.1016/j.chphma.2025.09.003](https://doi.org/10.1016/j.chphma.2025.09.003).

References

- [1] H.A. Maddah, Polypropylene as a promising plastic: A review, *Am. J. Polym. Sci.* 6 (2016) 1–11, doi:10.5923/j.ajps.20160601.01.
- [2] K. Shirvanimoghaddam, K.V. Balaji, R. Yadav, O. Zabihi, M. Ahmadi, P. Ade-tunji, M. Naebe, Balancing the toughness and strength in polypropylene composites, *Compos. Part B Eng.* 223 (2021) 109121, doi:10.1016/j.compositesb.2021.109121.
- [3] G. Zhang, C. Nam, T.C.M. Chung, L. Petersson, H. Hillborg, Polypropylene copolymer containing cross-linkable antioxidant moieties with long-term stability under elevated temperature conditions, *Macromolecules* 50 (2017) 7041–7051, doi:10.1021/acs.macromol.7b01235.
- [4] C. DeArmitt, Functional fillers for plastics, in: *Appl. Plast. Eng. Handb.*, Elsevier, 2011, pp. 455–468, doi:10.1016/B978-1-4377-3514-7.10026-1.
- [5] A. Fajdek-Bieda, A. Wróblewska, The use of natural minerals as reinforcements in mineral-reinforced polymers: A review of current developments and prospects, *Polymers (Basel)* 16 (2024) 2505, doi:10.3390/polym16172505.
- [6] J.H. Braun, A. Baidins, R.E. Marganski, TiO₂ pigment technology: A review, *Prog. Org. Coatings* 20 (1992) 105–138, doi:10.1016/0033-0655(92)80001-D.
- [7] P. Supaphol, P. Thanomkiat, J. Junkasem, R. Dangtungee, Non-isothermal melt-crystallization and mechanical properties of titanium(IV) oxide nanoparticle-filled isotactic polypropylene, *Polym. Test.* 26 (2007) 20–37, doi:10.1016/j.polymertesting.2006.07.011.
- [8] S. Wacharawichanant, S. Thongyai, T. Siripattanasak, T. Tipsri, Effect of mixing conditions and particle sizes of titanium dioxide on mechanical and morphological properties of polypropylene/titanium dioxide composites, *Iran. Polym. J.* 18 (2009) 607–616 <https://www.magiran.com/p653582>.
- [9] Y. Akinay, I.Nuri Akkuş, Synthesis and characterization of the pearlescent pigments based on mica deposited with SiO₂, AlN and TiO₂: First report of its dielectric properties, *Ceram. Int.* 46 (2020) 17735–17740, doi:10.1016/j.ceramint.2020.04.078.
- [10] M. Jahed-Jaafargolikhanlo, A. Habibi-Yangjeh, K. Pournemati, Y. Akinay, QDs-sized TiO_{2-x}/Bi₁₂O₁₅Cl₆/BiOCl photocatalysts with tandem n-n heterojunctions: Facile fabrication and impressive visible-light-induced photocatalytic performances, *Surf. Interfaces* 41 (2023) 103215, doi:10.1016/j.surfint.2023.103215.
- [11] M. Forhad Mina, S. Seema, R. Matin, M. Jellur Rahaman, R. Bijoy Sarker, M. Abdul Gafur, M. Abu Hashan Bhuiyan, Improved performance of isotactic polypropylene/titanium dioxide composites: Effect of processing conditions and filler content, *Polym. Degrad. Stab.* 94 (2009) 183–188, doi:10.1016/j.polymdegradstab.2008.11.006.
- [12] S.K. Esthappan, S.K. Kuttappan, R. Joseph, Effect of titanium dioxide on the thermal ageing of polypropylene, *Polym. Degrad. Stab.* 97 (2012) 615–620, doi:10.1016/j.polymdegradstab.2012.01.006.
- [13] S.K. Esthappan, S.K. Kuttappan, R. Joseph, Thermal and mechanical properties of polypropylene/titanium dioxide nanocomposite fibers, *Mater. Des.* 37 (2012) 537–542, doi:10.1016/j.matdes.2012.01.038.
- [14] S. Wang, A. Aji, S. Guo, C. Xiong, Preparation of microporous polypropylene/titanium dioxide composite membranes with enhanced electrolyte uptake capability via melt extruding and stretching, *Polymers* 9 (2017) 110, doi:10.3390/polym9030110.
- [15] D. Aydemir, G. Uzun, H. Gumuş, S. Yildiz, S. Gumuş, T. Bardak, G. Gunduz, Nanocomposites of polypropylene/nano titanium dioxide: Effect of loading rates of nano titanium dioxide, *Mater. Sci.* 22 (2016) 364–369, doi:10.5755/j01.ms.22.3.8217.
- [16] M. Peña-Juárez, G. Palestino-Escobedo, J. Navarrete-Damian, C.M. Del Angel-Olarte, C. Zarate-Orduño, L.A. Flores-Gonzalez, E.F. Armendáriz-Alonso, J.A. Gonzalez-Calderon, Water-mediated chelation dynamics of dicarboxylic acid functionalized TiO₂ nanoparticles for β -nucleation enhancement in isotactic polypropylene composites, *Polym. Technol. Mater.* 63 (2024) 2549–2562, doi:10.1080/25740881.2024.2377301.
- [17] R. Kumar, S.K. Mishra, U. Raj, S. Sengupta, R. Chatterjee, S. Pandey, S.M.M. Hasnain, A.E. Ragab, A.F. Deifalla, S. Jayapalan, Influence of graphene nanoplatelets (GnPs) and titanium dioxide (TiO₂) hybrid fillers on the mechanical, thermal, and morphological performance of polypropylene (PP) based hybrid composites, *Polym. Polym. Compos.* 32 (2024) 09673911241260160, doi:10.1177/09673911241260160.
- [18] H. Junaedi, M. Baig, A. Dawood, E. Albahkali, A. Almajid, Effect of the matrix melt flow index and fillers on mechanical properties of polypropylene-based composites, *Materials* 15 (2022) 7568, doi:10.3390/ma15217568.
- [19] J. Dong, Y. Tang, A. Nzihou, Y. Chi, Key factors influencing the environmental performance of pyrolysis, gasification and incineration waste-to-energy technologies, *Energy Convers. Manag.* 196 (2019) 497–512, doi:10.1016/j.enconman.2019.06.016.
- [20] N.R. Schwartz, A.D. Paulsen, M.J. Blaise, A.L. Wagner, P.E. Yelvington, Analysis of emissions from combusting pyrolysis products, *Fuel* 274 (2020) 117863, doi:10.1016/j.fuel.2020.117863.
- [21] J.A. Caballero, R. Font, M.M. Esperanza, Kinetics of the thermal decomposition of tannery waste, *J. Anal. Appl. Pyrolysis* 47 (1998) 165–181, doi:10.1016/S0165-2370(98)00081-3.
- [22] I. Martín-Gullón, M. Esperanza, R. Font, Kinetic model for the pyrolysis and combustion of poly-(ethylene terephthalate) (PET), *J. Anal. Appl. Pyrolysis* 58–59 (2001) 635–650, doi:10.1016/S0165-2370(00)00141-8.
- [23] P. Das, P. Tiwari, Thermal degradation kinetics of plastics and model selection, *Thermochim. Acta.* 654 (2017) 191–202, doi:10.1016/j.tca.2017.06.001.
- [24] X. Ren, Z. Huang, Pyrolysis of milk bottle wastes of polypropylene and high density polyethylene: determination of kinetic and thermodynamic parameters, *Energy Sources, Part A* 46 (2024) 13723–13740, doi:10.1080/15567036.2020.1804488.

- [25] T.E. Motaung, S.V. Motloung, L.F. Koao, T.D. Malevu, E.C. Linganiso, A thermic effect on degradation kinetics of sugar cane bagasse polypropylene composites, *J. Compos. Sci.* 6 (2022) 123, doi:10.3390/jcs6050123.
- [26] E. Esmizadeh, C. Tzoganakis, T.H. Mekonnen, Degradation behavior of polypropylene during reprocessing and its biocomposites: Thermal and oxidative degradation kinetics, *Polymers* 12 (2020) 1627, doi:10.3390/polym12081627.
- [27] J.Z. Liang, J.Z. Wang, G.C.P. Tsui, C.Y. Tang, Thermal decomposition kinetics of polypropylene composites filled with graphene nanoplatelets, *Polym. Test.* 48 (2015) 97–103, doi:10.1016/j.polymertesting.2015.09.015.
- [28] P.K. Vimalathithan, C. Barile, C. Casavola, S. Arunachalam, M.G. Battisti, W. Friesenbichler, C.T. Vijayakumar, Thermal degradation kinetics of polypropylene/clay nanocomposites prepared by injection molding compounder, *Polym. Compos.* 40 (2019) 3634–3643, doi:10.1002/pc.25226.
- [29] K. Chrissafis, K.M. Paraskevopoulos, S.Y. Stavrev, A. Docoslis, A. Vassiliou, D.N. Bikiaris, Characterization and thermal degradation mechanism of isotactic polypropylene/carbon black nanocomposites, *Thermochim. Acta.* 465 (2007) 6–17, doi:10.1016/j.tca.2007.08.007.
- [30] B. Lecouvet, S. Bourbigot, M. Sclavons, C. Bailly, Kinetics of the thermal and thermo-oxidative degradation of polypropylene/halloysite nanocomposites, *Polym. Degrad. Stab.* 97 (2012) 1745–1754, doi:10.1016/j.polymdegradstab.2012.06.022.
- [31] C.M. Guldberg, P. Waage, Über die chemische affinität, *J. Prakt. Chem.* 127 (1879) 69–114, doi:10.1002/prac.18790190111.
- [32] S. Arrhenius, Über die reaktionsgeschwindigkeit bei der inversion von rohrzucker durch säuren, *Zeitschrift Für Phys. Chemie.* 4 (1889) 226–248, doi:10.1515/zpch-1889-0416.
- [33] A.K. Galwey, Is the science of thermal analysis kinetics based on solid foundations? *Thermochim. Acta.* 413 (2004) 139–183, doi:10.1016/j.tca.2003.10.013.
- [34] H.L. Friedman, Kinetics of thermal degradation of char-forming plastics from thermogravimetry. Application to a phenolic plastic, *J. Polym. Sci. Part C Polym. Symp.* 6 (1964) 183–195, doi:10.1002/polc.5070060121.
- [35] T. Akahira, T. Sunose, Method of determining activation deterioration constant of electrical insulating materials, *Res. Rep. Chiba Inst. Technol.* 16 (1971) 22–31.
- [36] M.J. Starink, A new method for the derivation of activation energies from experiments performed at constant heating rate, *Thermochim. Acta.* 288 (1996) 97–104, doi:10.1016/S0040-6031(96)03053-5.
- [37] J.H. Flynn, L.A. Wall, A quick, direct method for the determination of activation energy from thermogravimetric data, *J. Polym. Sci. Part B Polym. Lett.* 4 (1966) 323–328, doi:10.1002/pol.1966.110040504.
- [38] J.H. Flynn, The isoconversional method for determination of energy of activation at constant heating rates, *J. Therm. Anal.* 27 (1983) 95–102, doi:10.1007/BF01907325.
- [39] J.H. Flynn, A general differential technique for the determination of parameters for $d(\alpha)/dt=f(\alpha)A \exp(-E/RT)$, *J. Therm. Anal.* 37 (1991) 293–305, doi:10.1007/BF02055932.
- [40] H.H. Horowitz, G. Metzger, A new analysis of thermogravimetric traces, *Anal. Chem.* 35 (1963) 1464–1468, doi:10.1021/ac60203a013.
- [41] A.W. Coats, J.P. Redfern, Thermogravimetric analysis. A review, *Analyst* 88 (1963) 906, doi:10.1039/an9638800906.
- [42] W.W. Wendlandt, Thermal methods of analysis, in: T.S. West (Ed.), *Phys. Chem. Ser. One, Phys. Chem. Ser. One*, 13, Baltimore University Park Press, 1973, pp. 177–200. <https://www.osti.gov/biblio/4533886>. *Anal. Chem. Part 2.*
- [43] M. Pijolat, L. Favergeon, Kinetics and mechanisms of solid-gas reactions, in: *Handb. Therm. Anal. Calorim.*, Elsevier, 2018, pp. 173–212, doi:10.1016/B978-0-444-64062-8.00011-5.
- [44] J.M. Criado, Kinetic analysis of DTG data from master curves, *Thermochim. Acta.* 24 (1978) 186–189, doi:10.1016/0040-6031(78)85151-X.
- [45] S. Vyazovkin, K. Chrissafis, M.L. Di Lorenzo, N. Koga, M. Pijolat, B. Roudit, N. Sbirrazzuoli, J.J. Suñol, ICTAC Kinetics Committee recommendations for collecting experimental thermal analysis data for kinetic computations, *Thermochim. Acta.* 590 (2014) 1–23, doi:10.1016/j.tca.2014.05.036.
- [46] A. Pratap, T. Lilly Shanker Rao, K.N. Lad, H.D. Dhurandhar, Isoconversional vs. Model fitting methods, *J. Therm. Anal. Calorim.* 89 (2007) 399–405, doi:10.1007/s10973-006-8160-7.
- [47] H.W. Cui, J.T. Jiu, T. Sugahara, S. Nagao, K. Sukanuma, H. Uchida, K.A. Schroder, Using the Friedman method to study the thermal degradation kinetics of photonicallly cured electrically conductive adhesives, *J. Therm. Anal. Calorim.* 119 (2015) 425–433, doi:10.1007/s10973-014-4195-3.
- [48] S.M. Al-Salem, B.K. Sharma, A.R. Khan, J.C. Arnold, S.M. Alston, S.R. Chandrasekaran, A.T. Al-Dhafeeri, Thermal degradation kinetics of virgin polypropylene (PP) and PP with starch blends exposed to natural weathering, *Ind. Eng. Chem. Res.* 56 (2017) 5210–5220, doi:10.1021/acs.iecr.7b00754.
- [49] P. Paik, K.K. Kar, Thermal degradation kinetics and estimation of lifetime of polyethylene particles: Effects of particle size, *Mater. Chem. Phys.* 113 (2009) 953–961, doi:10.1016/j.matchemphys.2008.08.075.
- [50] E. Galiwango, H. A.Gabbar, Synergistic interactions, kinetic and thermodynamic analysis of co-pyrolysis of municipal paper and polypropylene waste, *Waste Manag.* 146 (2022) 86–93, doi:10.1016/j.wasman.2022.04.032.
- [51] K. Pielichowski, J. Njuguna, T.M. Majka, Thermal Degradation of Polymeric Materials, Second Edi, Elsevier, 2023, doi:10.1016/C2019-0-04932-1.
- [52] A. Zohrevand, A. Ajji, F. Mighri, Morphology and properties of highly filled iPP/TiO₂ nanocomposites, *Polym. Eng. Sci.* 54 (2014) 874–886, doi:10.1002/pen.23625.
- [53] R. Sharma, S.N. Maiti, Effects of crystallinity of polypropylene (PP) on the mechanical properties of PP/styrene-ethylene-butylene-styrene-g-maleic anhydride (SEBS-g-MA)/teak wood flour (TWF) composites, *Polym. Bull.* 72 (2015) 627–643, doi:10.1007/s00289-014-1296-x.
- [54] S.N. Maiti, K. Ghosh, Thermal characteristics of silver powder-filled polypropylene composites, *J. Appl. Polym. Sci.* 52 (1994) 1091–1103, doi:10.1002/app.1994.070520810.
- [55] S.S. Ray, M. Okamoto, Polymer/layered silicate nanocomposites: A review from preparation to processing, *Prog. Polym. Sci.* 28 (2003) 1539–1641, doi:10.1016/j.progpolymsci.2003.08.002.
- [56] J.A. Gonzalez-Calderon, J.C. Fierro-Gonzalez, M.G. Peña-Juarez, E. Perez, A. Almdendez-Camarillo, Influence of the chemical functionalization of titanium oxide nanotubes on the non-isothermal crystallization of polypropylene nanocomposites, *J. Mater. Sci.* 57 (2022) 5855–5872, doi:10.1007/s10853-022-07009-x.
- [57] I.L. Soares, J.P. Chimanowsky, L. Luetkemeyer, E.O. da Silva, D. de H.S. Souza, M.I.B. Tavares, Evaluation of the influence of modified TiO₂ particles on polypropylene composites, *J. Nanosci. Nanotechnol.* 15 (2015) 5723–5732, doi:10.1166/jnn.2015.10041.
- [58] B. Suksut, Morphology and Morphology Formation of Injection Molded PP-based Nanocomposites, Technische Universität Kaiserslautern, 2016 https://kluedo.uni-rptu.de/frontdoor/deliver/index/docId/4433/file/Dissertation_Buncha_Suksut.pdf.
- [59] N. Sbirrazzuoli, Is the Friedman method applicable to transformations with temperature dependent reaction heat? *Macromol. Chem. Phys.* 208 (2007) 1592–1597, doi:10.1002/macp.200700100.
- [60] J. Wang, X. Cai, Kinetics study of thermal oxidative degradation of ABS containing flame retardant components, *J. Therm. Anal. Calorim.* 107 (2012) 725–732, doi:10.1007/s10973-011-1704-5.
- [61] S. Sukarni, A.A. Putra, A. Prasetyo, Y. Zakaria, A.Y. Aminullah, A.A. Permasari, P. Puspitasari, Horowitz-Metzger kinetic analysis of coconut shell waste combustion using thermogravimetric technique, in: *AIP Conf. Proc.*, AIP Publishing, 2024, 070003, doi:10.1063/5.0228173.
- [62] A.A.M. Aly, A.H. Osman, M.A. EL-Mottaleb, G.A.H. Gouda, Thermal stability and kinetic studies of cobalt (II), nickel (II), copper (II), cadmium (II) and mercury (II) complexes derived from n-salicylidene Schiff bases, *J. Chil. Chem. Soc.* 54 (2009) 349–353, doi:10.4067/S0717-97072009000400005.
- [63] H. Mahmood, A. Raza, M. Raashid, A. Khan, S. Mehmood, Comparative impact of acidified glycerol pretreatment on the thermal degradation kinetics of crude wheat straw for potential sustainable valorization, *React. Kinet. Mech. Catal.* 138 (2025) 1409–1425, doi:10.1007/s11144-024-02790-z.
- [64] L. Vlaev, N. Nedelchev, K. Gyurova, M. Zagorcheva, A comparative study of non-isothermal kinetics of decomposition of calcium oxalate monohydrate, *J. Anal. Appl. Pyrolysis.* 81 (2008) 253–262, doi:10.1016/j.jaap.2007.12.003.
- [65] A. Aboulkas, K. El harfi, A. El Bouadili, Thermal degradation behaviors of polyethylene and polypropylene. Part I: Pyrolysis kinetics and mechanisms, *Energy Convers. Manag.* 51 (2010) 1363–1369, doi:10.1016/j.enconman.2009.12.017.
- [66] A.W. Coats, J.P. Redfern, Kinetic parameters from thermogravimetric data, *Nature* 201 (1964) 68–69, doi:10.1038/201068a0.
- [67] A.W. Coats, J.P. Redfern, Kinetic parameters from thermogravimetric data. II, *J. Polym. Sci. Part B Polym. Lett.* 3 (1965) 917–920, doi:10.1002/pol.1965.110031106.
- [68] S. Vyazovkin, A.K. Burnham, J.M. Criado, L.A. Pérez-Maqueda, C. Popescu, N. Sbirrazzuoli, ICTAC Kinetics Committee recommendations for performing kinetic computations on thermal analysis data, *Thermochim. Acta.* 520 (2011) 1–19, doi:10.1016/j.tca.2011.03.034.
- [69] N. Karimpour-Motlagh, H.A. Khonakdar, S.H. Jafari, M. Panahi-Sarmad, A. Javadi, S. Shojaei, V. Goodarzi, An experimental and theoretical mechanistic analysis of thermal degradation of polypropylene/poly(lactic acid)/clay nanocomposites, *Polym. Adv. Technol.* 30 (2019) 2695–2706, doi:10.1002/pat.4699.
- [70] A. Prasetyo, Sukarni, P. Puspitasari, The Coats-Redfern models kinetics analysis of tetraselmis Chuii—Titanium dioxide nanoparticle blend during combustion process, in: *Recent Adv. Mech. Eng. Sel. Proc. ICOMET 2021*, Springer, 2023, pp. 273–281, doi:10.1007/978-981-19-0867-5_33.
- [71] N. Fatemi, R. Whitehead, D. Price, D. Dollimore, Some comments on the use of Avrami-Erofeev expressions and solid state decomposition rate constants, *Thermochim. Acta.* 104 (1986) 93–100, doi:10.1016/0040-6031(86)85187-5.
- [72] K. Shirzad, C. Viney, A critical review on applications of the Avrami equation beyond materials science, *J. R. Soc. Interface.* 20 (2023) 20230242, doi:10.1098/rsif.2023.0242.
- [73] A. Ortega, L.A. Pérez-Maqueda, J.M. Criado, Simultaneous determination of the activation energy and the reaction kinetic model from the analysis of a single curve obtained by a novel method, *J. Therm. Anal.* 42 (1994) 551–557, doi:10.1007/BF02548535.